minerals

MDPI

Article

Occurrence and Distribution of Moganite and Opal-CT in Agates from Paleocene/Eocene Tuffs, El Picado (Cuba)

Jens Götze [1,*], Klaus Stanek [2], Gerardo Orozco [3], Moritz Liesegang [4] and Tanja Mohr-Westheide [5]

[1] Institute for Mineralogy, TU Bergakademie Freiberg, Brennhausgasse 14, 09599 Freiberg, Germany
[2] Institute for Geology, TU Bergakademie Freiberg, Cottastraße 4, 09599 Freiberg, Germany; klaus-peter.stanek@geo.tu-freiberg.de
[3] Departamento de Geología, Universidad de Moa, Avenida Calixto Garcia Iñiguez 15, Moa, Holguín 83330, Cuba; orozcog49@gmail.com
[4] Institute for Geological Sciences, FU Berlin, Malteserstraße 74–100, 12249 Berlin, Germany; m.liesegang@fu-berlin.de
[5] Institute for Evolution and Biodiversity Science, Museum für Naturkunde, Invalidenstraße 43, 10115 Berlin, Germany; Tanja.Mohr-Westheide@mfn-berlin.de
* Correspondence: jens.goetze@mineral.tu-freiberg.de

Abstract: Agates in Paleocene/Eocene tuffs from El Picado/Los Indios, Cuba were investigated to characterize the mineral composition of the agates and to provide data for the reconstruction of agate forming processes. The volcanic host rocks are strongly altered and fractured and contain numerous fissures and veins mineralized by quartz and chalcedony. These features indicate secondary alteration and silicification processes during tectonic activities that may have also resulted in the formation of massive agates. Local accumulation of manganese oxides/hydroxides, as well as uranium (uranyl), in the agates confirm their contemporaneous supply with SiO_2 and the origin of the silica-bearing solutions from the alteration processes. The mineral composition of the agates is characterized by abnormal high bulk contents of opal-CT (>6 wt%) and moganite (>16 wt%) besides alpha-quartz. The presence of these elevated amounts of "immature" silica phases emphasize that agate formation runs through several structural states of SiO_2 with amorphous silica as the first solid phase. A remarkable feature of the agates is a heterogeneous distribution of moganite within the silica matrix revealed by micro-Raman mapping. The intensity ratio of the main symmetric stretching-bending vibrations (A_1 modes) of alpha-quartz at 465 cm^{-1} and moganite at 502 cm^{-1}, respectively, was used to depict the abundance of moganite in the silica matrix. The zoned distribution of moganite and variations in the microtexture and porosity of the agates indicate a multi-phase deposition of SiO_2 under varying physico-chemical conditions and a discontinuous silica supply.

Keywords: agate; alpha-quartz; chalcedony; moganite; opal-CT; Raman spectroscopy

Citation: Götze, J.; Stanek, K.; Orozco, G.; Liesegang, M.; Mohr-Westheide, T. Occurrence and Distribution of Moganite and Opal-CT in Agates from Paleocene/Eocene Tuffs, El Picado (Cuba). *Minerals* **2021**, *11*, 531. https://doi.org/10.3390/min11050531

Academic Editor: Galina Palyanova

Received: 27 April 2021
Accepted: 12 May 2021
Published: 18 May 2021

1. Introduction

Cuba is a country that is particularly famous for its enormous deposits of Ni ores. Huge surficial laterite horizons in the eastern part of the Caribbean island belong to the most important nickel deposits in the world and contain considerable amounts of other valuable chemical compounds of, e.g., Sc, Co, or rare earth elements (REE) [1]. However, occurrences of other mineral deposits are rare and restricted to a few locations.

For instance, different gemstones were exploited between 1989 and 1998 in Cuba, especially silica minerals and rocks such as chalcedony, opal, jasper or silicites [2]. Remarkable are chalcedony from Palmira near Cienfuegos, opal from Loma de los Ópalos and Pontezuela (near Camagüey) as well as silicites from Corralillo on the northern coast of Cuba (Figure 1). Silicified wood occurs in Upper Cretaceous volcanic sequences of the Sierra de Najasa SE of Camagüey (Sibanicu) and above ophiolites in the Sierra de Cubitas north of Camagüey (Miocene) [2,3].

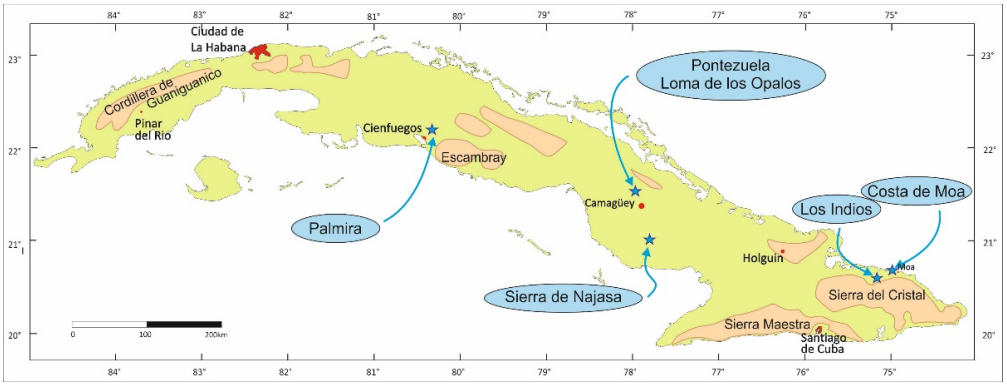

Figure 1. A geomorphological map of Cuba showing occurrences of different SiO_2 mineralization.

Agates were sporadically found in Upper Cretaceous rocks overlaying ophiolites of the Camagüey fault zone NE of Camagüey. In addition, chalcedony, jasper and silicified corals are reported from the Rio Yumuri region near Matanzas [2]. In the eastern part of Cuba, silica mineralization occurs in particular in the surrounding area of Moa. Jasper was found in altered serpentinites of the Costa de Moa region, whereas agates/chalcedony occur in altered volcanic rocks in the region of El Picado, W of Moa as well as near Baracoa on the river Toa, E of Moa (Figure 1).

Because of the lack of mineralogical data, the agates of the Moa region were in the focus of the present study. Mineralogical and geochemical investigations were aimed to characterize the silica minerals in the agates and to provide data for the reconstruction of agate formation processes in Moa. On the other hand, the results of the study should provide additional general arguments for the ongoing discussion concerning the enigma of agate genesis [3,4]. Emphasis was placed on the detection and distribution of the monoclinic silica polymorph moganite and opal-CT, which both occur in considerable amounts in the agates from the surroundings of Moa.

2. Geological Background and Sample Material

The geology of Cuba is dominated by metamorphic and sedimentary rocks. The geographic position in a tectonically active region, with plate movements in Mesozoic to Cenozoic times along NE trending fault systems, resulted in a geologic trisection [5]. The western part of the island is mainly characterized by carbonate sediments and widespread karst formation. The central part (Escambray) consists of ophiolites, lifted metamorphic rocks and carbonate sediments. The eastern part of Cuba is dominated by the largest ophiolite complexes of the Caribbean, K-poor volcanic rocks (and associated intrusive rocks) of the Paleogene to Eocene island arc volcanism, as well as overlaying calcareous sediments [5].

The investigated agate material derives from El Picado near the village of Los Indios, ca. 15 km west of the city of Moa (Figure 1). The host rocks are strongly altered Paleocene/Eocene tuffs (ca. 55 Ma) locally intercalated with limestones. The altered volcanic rocks are fractured and contain numerous fissures and veins mineralized by quartz and chalcedony, indicating a secondary silicification of the pyroclastic material during tectonic activities (Figure 2).

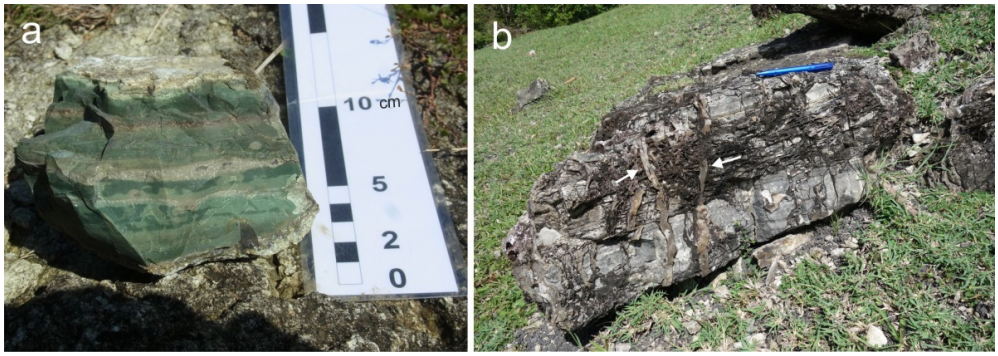

Figure 2. (**a**) A layered and strongly altered tuff and (**b**) a brecciated volcanic host rock with secondary quartz and chalcedony veins (arrows) from El Picado, Cuba.

XRD studies of the surrounding host rocks provided an average mineral composition of 8–10 wt% plagioclase (andesine), ca. 20 wt% dioctahedral illite-smectite mixed-layer minerals, 11–14 wt% zeolite (clinoptilolite), 6–8 wt% quartz, ca. 40 wt% opal-CT, and 10–12 wt% calcite. These results document that the primary mineral composition of the volcanic rocks is strongly modified during the alteration processes, resulting in the release of remarkable amounts of SiO_2.

The occurrence of agate in the investigation area around El Picado/Los Indios is variable. Agates appear both within the outcropping volcanic host rocks and as loose material surficially distributed in the field (Figure 3). Chalcedony shows different colors (white, grey, blue, yellow) and often collomorph or botryoidal habit (Figures 3a and 4c). Agates may occur in remarkable sizes but often exhibit only weak banding (Figures 3b and 4a,b).

Figure 3. (**a**) Chalcedony with botryoidal texture and (**b**) large yellow agate in weathered volcanic bedrock from El Picado, Cuba.

The collected sample material was documented and macroscopically described. Several agates were cut and polished to better visualize the agate textures. Finally, ten samples of different characteristics and textures were selected and prepared for detailed mineralogical investigations representing three main types (ACu1–3; Figure 4).

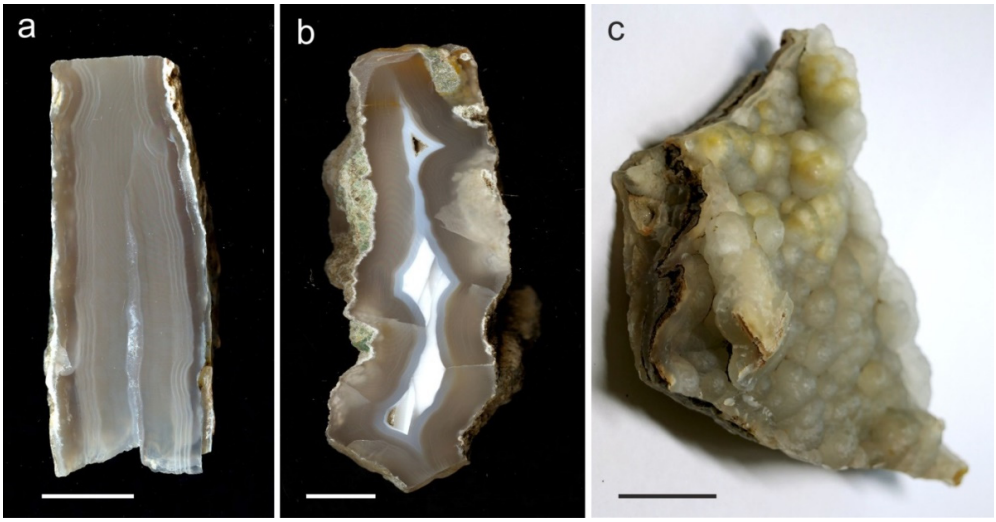

Figure 4. Selected samples of the investigated agate/chalcedony material from El Picado/Los Indios, Cuba representing three main types: (**a**) finely banded, vein-like agate (sample ACu1); (**b**) agate with a white center (ACu2); (**c**) botryoidal chalcedony (ACu3); the scale bar is 2 cm.

3. Analytical Methods

The mineral composition of the agates and volcanic host rocks was analyzed by X-ray diffraction (XRD) measurements on selected and prepared (<20 µm) sample material. The qualitative and quantitative phase compositions were analyzed using an URD 6 (Seifert/Freiberger Präzisionsmechanik) and a METEOR 0D Si drift detector (GE Sensing & Inspection Technologies GmbH, Ahrensburg, Germany) with Co Kα-radiation in the range of 5–80° (2θ). Analytical conditions included a detector slit of 0.25 mm, 0.03° step width and 5 s measuring time per step. Data evaluation was realized using the Analyse RayfleX v.2.352 software and subsequent Rietveld refinement with Autoquan v.2.7.00 [6].

The identification and characterization of different SiO_2 phases was performed by a combination of X-ray diffraction and Raman spectroscopy. Raman spectroscopy analyses were conducted on a Horiba Jobin Yvon LabRAM HR 800 instrument coupled to an Olympus BX41 microscope. For mappings, unpolarized spectra were collected with the LabSpec 6 software over a range from 90 to 600 cm^{-1} at a step size of 8 µm. A 633 nm laser was used to excite the sample with a 50× objective, at a spectral integration time of 5 s, and two accumulations. Scattered Raman light was collected in backscattering geometry and dispersed by a grating of 600 grooves/mm after passing through a 100 µm entrance slit. The confocal hole size was set to 1000 µm. An internal intensity correction (ICS, Horiba, Kyoto, Japan) was used to correct detector intensities. The instrument was calibrated using the Raman band of a silicon wafer at 520.7 cm^{-1}.

Microscopic investigations comprised an integrated analysis by polarizing, cathodoluminescence (CL) and scanning electron microscopy (SEM) on polished thin sections (30 µm). Conventional polarizing microscopy in transmitted light was conducted with a Zeiss Axio Imager A1m microscope. Additional Nomarski differential interference contrast (DIC) imaging in reflected light was performed using specific Nomarski DIC prisms to visualize variations of the surface topography.

These investigations were completed by SEM studies as well as CL analyses with an optical CL microscope HC1-LM on carbon-coated, polished thin sections [7]. The SEM measurements (SE, BSE), including local chemical analyses (EDX), were performed using a JEOL JSM-7001F (20 kV, 2.64 nA) with a BRUKER Quantax 800 EDX system. CL microscopy and spectroscopy were operated at 14 kV accelerating voltage and a current of 0.2 mA with a Peltier cooled digital video camera (OLYMPUS DP72) and an Acton Research SP-2356 digital triple-grating spectrograph with a Princeton Spec-10 CCD detector, respectively. CL spectra in the wavelength range from 380 to 900 nm were measured under standardized

conditions (wavelength calibration by a Hg-halogen lamp, spot width 30 µm, measuring time 5 s).

4. Results

4.1. Mineralogy and Microstructure of the Agates

The mineralogical composition of the agates from El Picado comprises different phases. In addition to microcrystalline (chalcedony) and macrocrystalline quartz, the agates contain elevated contents of moganite and opal-CT, as well as minor amounts of calcite (Table 1, Figure 5).

Table 1. The mineral composition (wt%) of agate samples from El Picado (Cuba) determined by X-ray diffraction measurements with Rietveld refinement.

	ACu1	ACu2	ACu3
α-quartz	89.1 ± 0.4	84.2 ± 0.4	74.4 ± 0.4
Moganite	10.9 ± 0.3	13.5 ± 0.3	16.8 ± 0.3
Opal-CT	-	2.2 ± 0.1	6.2 ± 0.1
Calcite	-	-	2.6 ± 0.1

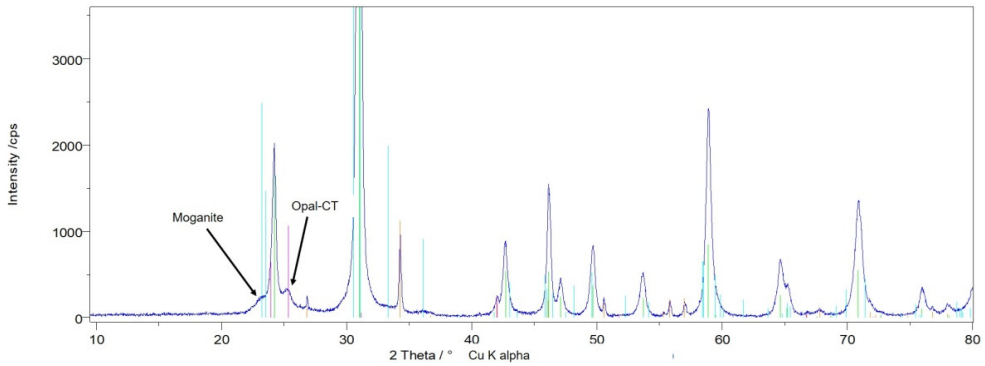

Figure 5. The X-ray diffraction pattern of sample ACub3 (powder sample, background corrected); search-match results in stick patterns: magenta, opal-CT (PDF 00-066-0177); light blue, moganite (PDF 01-073-2991); green, quartz (PDF 01-070-3755); red, calcite (PDF 01-083-0577). The arrows point to the characteristic broad maxima of moganite and opal-CT.

The microtexture of the agates is, in general, characterized by a sequence of granular, microcrystalline quartz, alternating layers of chalcedony with micro-granular quartz, fibrous chalcedony, and macrocrystalline quartz from the agate rim to the center (Figure 6a). In particular, the granular quartz layers are clearly distinguishable from chalcedony bands due to the varying porosity (Figure 6b). In contrast, the transition of fibrous chalcedony to macrocrystalline quartz in the center is smooth (Figure 6c).

The presence and spatial distribution of the silica polymorph moganite is difficult to detect by microscopic methods because of the similar optical properties and the narrow intergrowth with chalcedony. Although the moganite content in the agate samples from El Picado exceeds 10 wt% (compare Table 1), it was not possible to identify the monoclinic silica polymorph by polarizing or scanning electron microscopy. In contrast to moganite, opal-CT can be detected in the scanning electron microscope because of its specific morphological characteristics (Figure 7). Opal-CT forms typical lepispheres, spherical aggregates consisting of small crystal blades [8]. Local chemical analyses by SEM-EDX revealed elevated concentrations of Al (up to 0.55 wt%—see Figure 7b) in opal-CT. This contrasts with Al concentrations in chalcedony and macrocrystalline quartz (8–13 ppm) in the same agate samples [9].

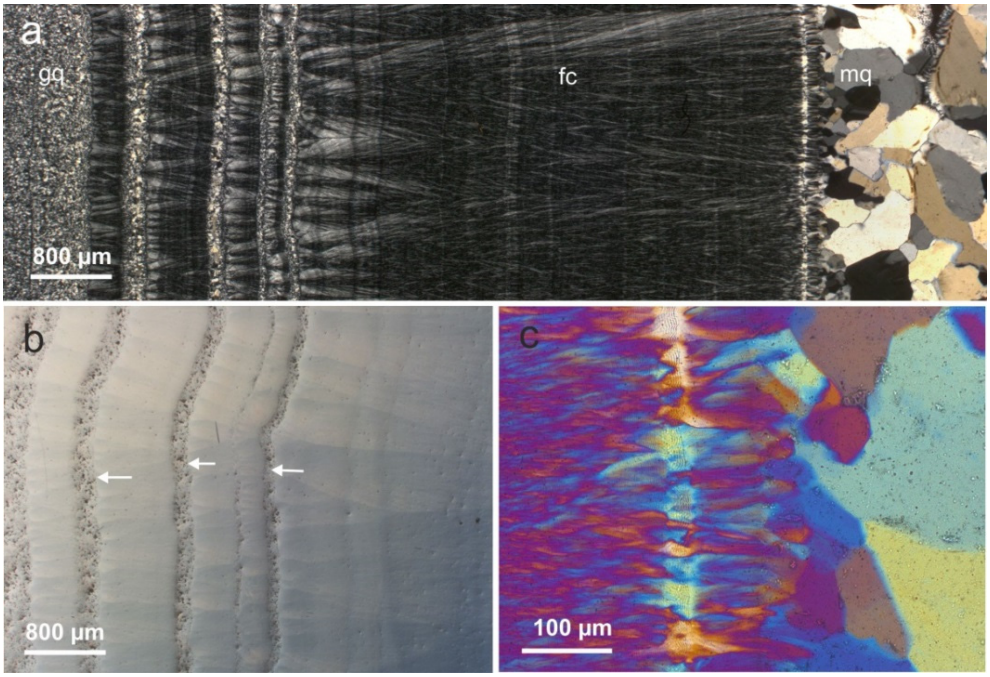

Figure 6. The microtexture of sample ACu1: (**a**) sequence of silica phases from the margin of the agate to the center with granular, microcrystalline quartz (gq), alternating layers of chalcedony with fine-grained quartz, fibrous chalcedony (fc) and macrocrystalline quartz (mq); (**b**) Nomarski DIC micrograph illustrating the differences in porosity between chalcedony and quartz layers; the surface relief imaged by Nomarski DIC microscopy reveals higher porosity in the micro-granular quartz layers (arrows); (**c**) micrograph in polarized light and additional nγ/λ-compensator showing the smooth transition from fibrous chalcedony to macrocrystalline quartz in the agate center.

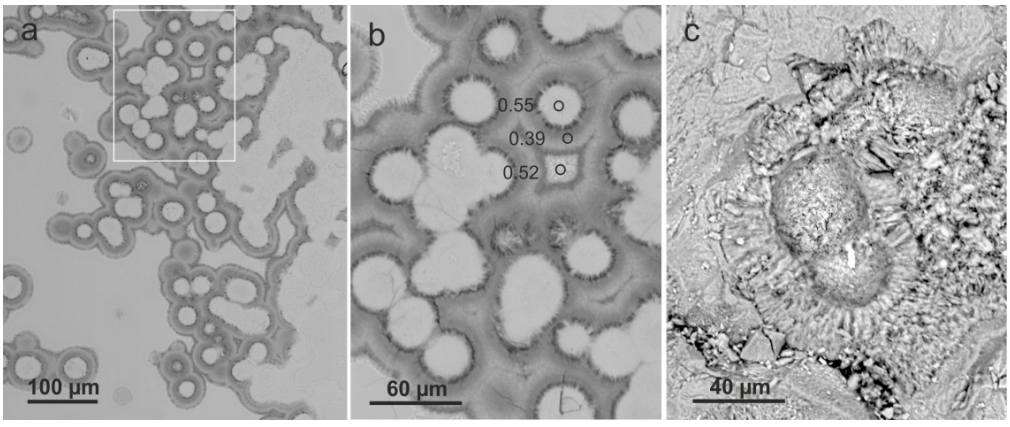

Figure 7. SEM-micrographs showing the appearance of opal-CT in agate sample ACu3: (**a**) a SEM-BSE image of the spherical opal-CT aggregates; (**b**) a close-up of (**a**) (see rectangle) with details and results of local chemical analyses of Al (in wt%) by SEM-EDX; (**c**) a SEM composite micrograph of opal-CT lepispheres revealing the characteristic spheres consisting of small crystal blades.

In addition to the different silica minerals, certain other phases were detected in the agates from El Picado. Calcite was detected in sample ACu3 in the contact area to the altered host rocks. The carbonate grains are partially corroded and replaced by silica minerals (Figure 8a); moreover, inclusions of dark material could be observed within the chalcedony matrix that is texturally arranged along the agate banding (Figure 8b). Local chemical analyses by SEM-EDX confirmed the presence of manganese oxides/hydroxides, which have probably been primarily intercalated into the SiO_2 matrix. According to local

chemical analyses by SEM-EDX, the Mn concentrations in the dark areas varied between 2.52 and 5.41 wt%.

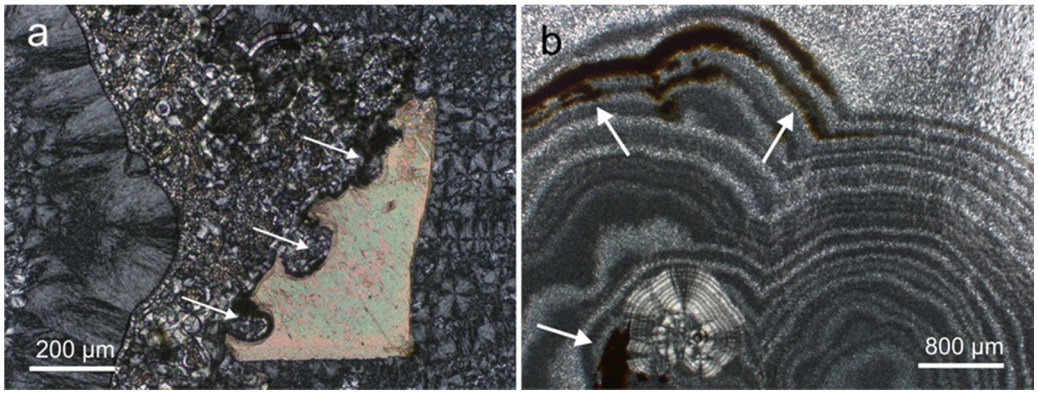

Figure 8. Micrographs in transmitted light (crossed polars) of non-silica phases in the agates from El Picado: (**a**) calcite grain (sample ACu3), which is partially corroded by SiO_2 (arrows); (**b**) intercalation of dark banded manganese oxides/hydroxides (sample ACu2) arranged along the chalcedony banding (see arrows) pointing to simultaneous accumulation and precipitation from mineralizing fluids.

4.2. Occurrence and Distribution of Moganite

Because of the limitations of microscopic techniques for the identification of moganite, Raman spectroscopy was used to provide information about the occurrence and spatial distribution of moganite in the agates from El Picado/Los Indios. Previous studies have shown that quartz and moganite can be distinguished due to their different spectral characteristics. The identification of the two silica polymorphs is possible by the characteristic main symmetric stretching–bending vibrations (A_1 modes) of alpha-quartz at 465 cm^{-1} and moganite at 502 cm^{-1}, respectively [10].

Point analyses in different areas of the El Picado agates revealed variations in the moganite-to-quartz ratio detectable by different intensities of the relevant peaks in the Raman spectra (Figure 9a). The analytical data indicate that the moganite content in the agates is not homogeneously distributed. There exist chalcedony bands with high contents of moganite as well as bands without—more or less—any moganite. This conclusion confirms previous results, which documented the variations in moganite content in different parts of agates and even within the chalcedony banding [11–13].

In continuation of the local Raman spectroscopic analyses, Raman mapping was performed to provide detailed information about the semi-quantitative spatial distribution of moganite in the agates. The integral ratio of the 502/465 cm^{-1} Raman bands of moganite and quartz, respectively, was used to depict the abundance of moganite in the silica matrix. Figure 8b illustrates a heterogeneous distribution of moganite in the agate, which strongly correlates with the structural banding; however, moganite content may even fluctuate within individual fibrous chalcedony layers. Considering the average moganite contents detected with XRD (Table 1), the local moganite content in moganite-rich areas must be significantly higher than 15 wt%.

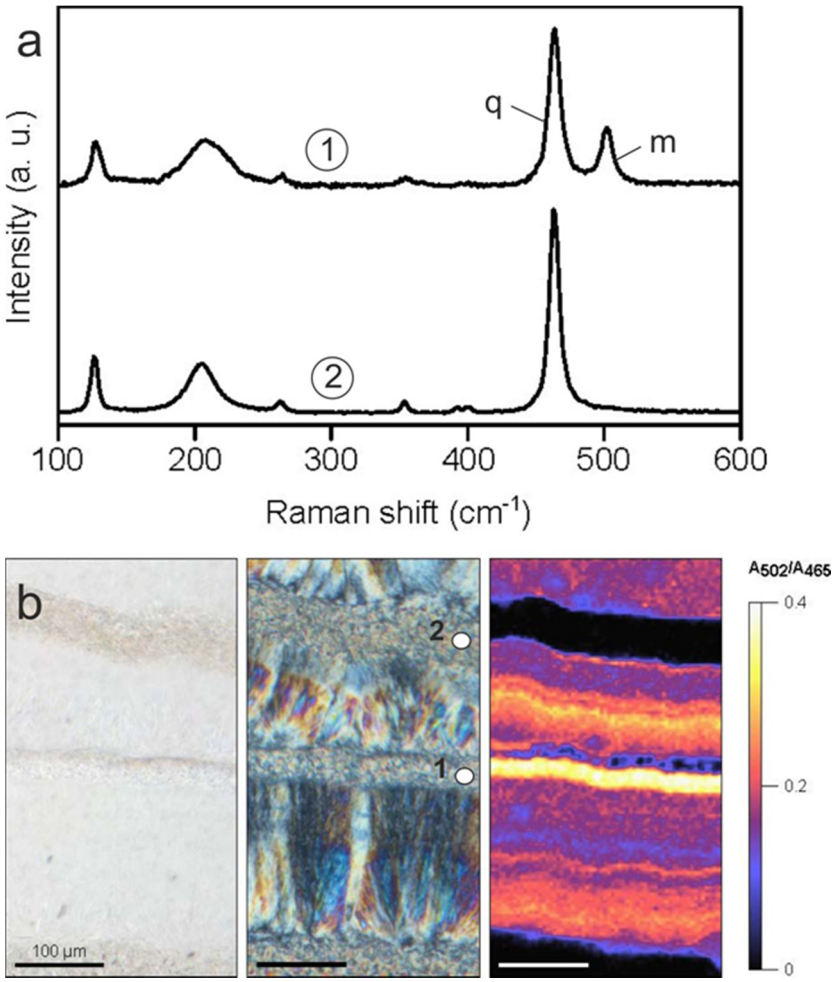

Figure 9. Results of Raman spectroscopy and Raman mapping of agate sample ACu1: (**a**) Raman spectra of two local analyses in different agate areas (compare b); spectrum 1 shows the characteristic main symmetric stretching-bending vibrations (A_1 modes) of alpha-quartz (q) at 465 cm^{-1} and moganite (m) at 502 cm^{-1}, respectively; whereas spectrum 2 shows only the band of alpha-quartz; (**b**) agate area in transmitted light with parallel and crossed polars, respectively, and the related Raman map based on the integral ratio of the 502/465 cm^{-1} bands; high ratios (yellow) point to areas with high moganite content.

4.3. Cathodoluminescence (CL) Properties of the Agates

CL microscopy and spectroscopy of the agates illustrate relatively uniform CL properties, exemplarily shown for ACu2 in Figure 10. The visible CL color is mostly a greenish-blue turning into a reddish-brown during electron irradiation (Figure 10a,b). Spectral CL measurements revealed a complex emission consisting of a broad composite blue band and a strong emission band centered at ca. 650 nm (Figure 10d). In addition, multiple emission peaks between 500 and 600 nm can be related to the luminescence of the UO_2^{2+} uranyl ion [14]. This greenish luminescence signal is characterized by a typical emission line at ~500 nm accompanied by several equidistant lines due to the harmonic vibrations of oxygen atoms in the uranyl complex (Figure 10d).

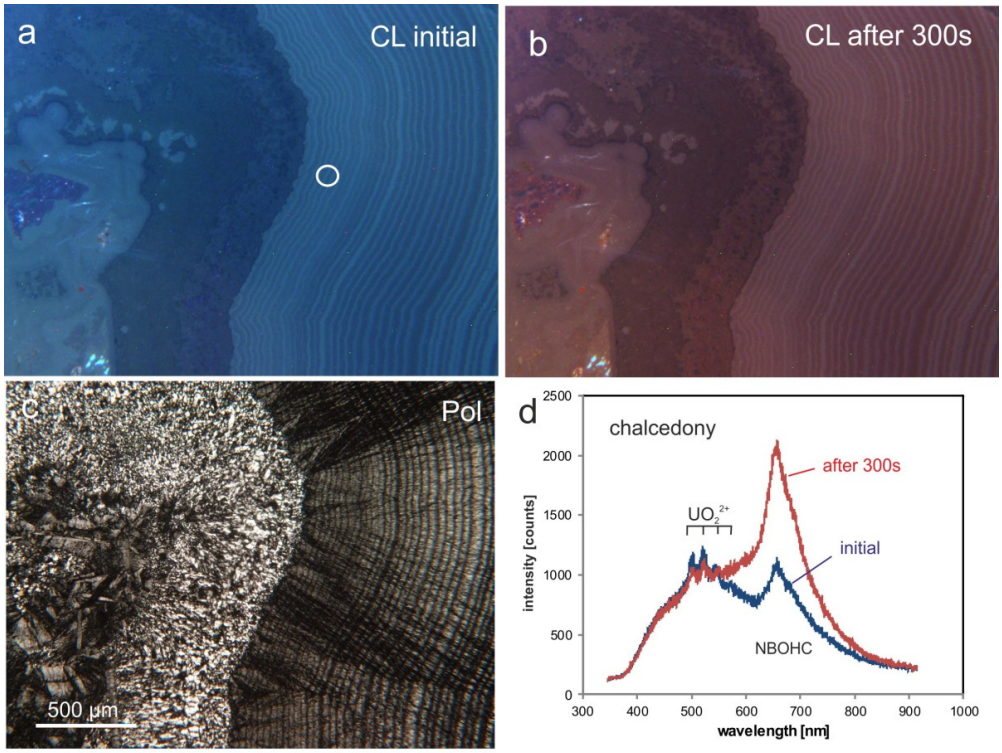

Figure 10. Micrographs of agate ACu2 showing the initial CL (**a**) compared with the CL after 300 s electron irradiation (**b**) and the sample area in transmitted light (crossed polars) (**c**) as well as the related CL spectra, which are dominated by a strong emission band centered at ca. 650 nm due to the non-bridging oxygen hole center (NBOHC) and multiple emission lines of the uranyl ion (**d**). The circle in (**a**) marks the position of the spectral CL measurement.

The 650 nm band (1.91 eV) is the most common CL emission in chalcedony and can be related to the non-bridging oxygen hole center (NBOHC) [15]. Whereas the broad blue emission is relatively stable under the electron beam, the 650 nm emission is very sensitive to electron irradiation, resulting in an increase in the band intensity during electron bombardment due to the conversion of different precursors (e.g., silanol groups: Si–O–H, Na impurities: Si–O–Na) into hole centers [16]. This is detectable by a change of the visible CL color from a greenish-blue to a reddish-brown (Figure 10a,b).

In contrast to the common CL behavior of most agates, the opal-CT rich parts of sample ACu3 exhibit a quite contrasting luminescence behavior (Figure 11). The visible luminescence color is bright blue and spectral measurements reveal a dominating broad band at ca. 500 nm, whereas the 650 nm emission band is subordinate. Such luminescence spectra were found in amorphous silica samples such as opal and opal-CT [17].

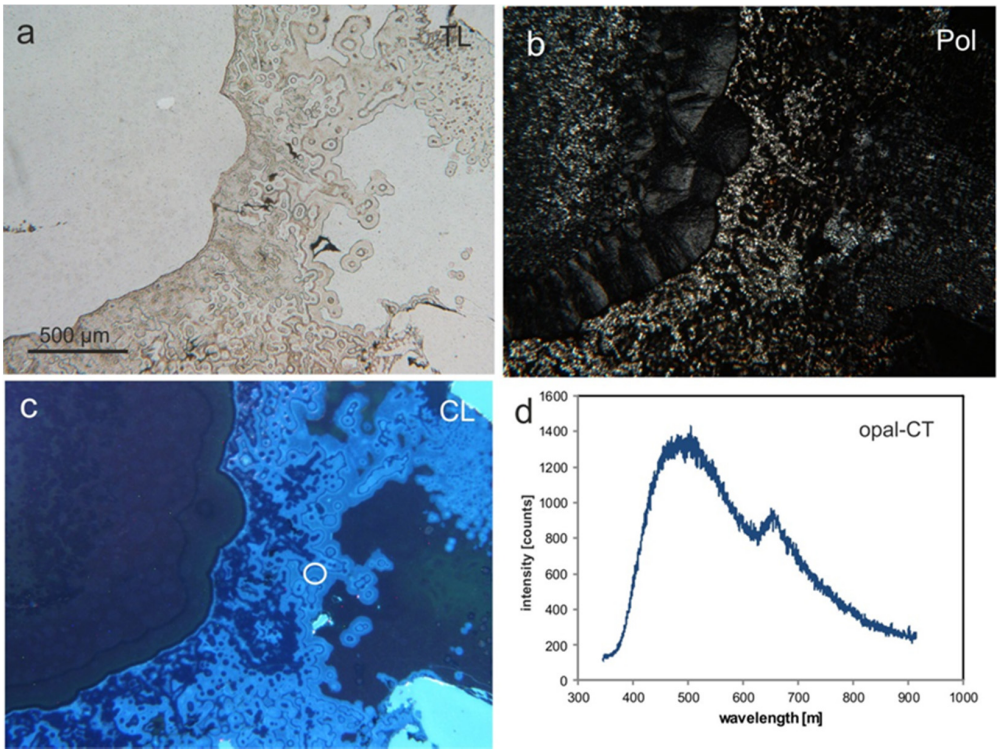

Figure 11. Micrographs of agate ACu3 in transmitted light (**a**) with crossed polars (**b**) and CL mode (**c**) showing the CL of an opal-CT rich area with a bright blue CL. (**d**) The related CL spectrum is dominated by a broad band centered around 500 nm; the circle in (**c**) marks the position of the spectral CL measurement.

5. Discussion

The discussion concerning the formation of agates in the Paleocene/Eocene tuffs from El Picado first focusses on the question about the origin of silica. Both the geological conditions of exposure of the volcanic rocks observed during field work and their mineralogical composition point to strong secondary alteration processes. The XRD results document high amounts of dioctahedral illite-smectite mixed-layer minerals and zeolites as typical alteration products of basic volcanic rocks. The primary mineral composition of the agate-bearing volcanic rocks is strongly modified, containing only residual plagioclase from the original inventory. These alteration processes must have caused the release of remarkable amounts of SiO_2 that have been available for silicification processes and the formation of massive agates. The SiO_2 supply is thereby associated with hydrothermal activities and secondary alteration of the predominantly SiO_2-poor, basic rocks.

Further indications concerning the formation processes were provided by previous investigations of fluid inclusions in macrocrystalline quartz crystals in the agates. Measured homogenization temperatures of aqueous inclusions scatter in a narrow range between 130 and 145 °C [7], emphasizing a source from low temperature hydrothermal solutions and/or heated meteoric water.

The detection of uranyl ions in the silica matrix by CL spectroscopy is another indication of intensive alteration processes. Uranium might be released from volcanic rocks during alteration processes and accumulated together with silica [18]. In result, uranium can be adsorbed from solution by natural silica compounds (silica colloids) and then trapped as a uranyl–silicate complex in a stable silica matrix [19]. A substitution of Si ions in the quartz lattice by U is unlikely due to the different crystal–chemical properties. The CL studies confirm the existence of uranyl compounds in quartz and chalcedony of agates, as it was already found in agates from other locations [14]. This binding mechanism of uranyl–silicate complexes in microcrystalline SiO_2 suggests a new mechanism of U deposition involving uranyl co-precipitation with silica during alteration processes.

Both field observations, concerning the appearance of agates in the host rocks and their mineralogical characteristics, illustrate that agates in El Picado can mostly be related to the crystallization from silica-rich solutions in fissures and cavities of the volcanic host rocks. The presence of opal-CT as an intermediate silica phase between amorphous and crystalline SiO_2 is a strong indication that the agate formation processes started from non-crystalline silica; particularly, in geologically young volcanic host rocks worldwide, opal-CT is detectable, since it has not been completely transformed to quartz [20,21]. Therefore, the preservation of opal-CT in the Cuban agates can be explained by the relatively young age (~55 Ma) of the hosting tuff layers.

The same applies for the unstable monoclinic SiO_2-modification moganite. A correlation between the formation age of the agates and the corresponding moganite content was first published by Moxon and Rios [22]. The amount of moganite in the agates strongly decreases with increasing age. For instance, less than 6 wt% moganite in agates from six 300 to 1100 Ma old host rocks was measured [23]; agates from a further three locations contained even less than 1 wt% moganite. In addition, Moxon [24,25] proved that the conversion of metastable silica phases into quartz is accompanied by loss of structural water and the coarsening of crystallite size.

The analyses of the present study emphasize that the agates from El Picado contain more than 15 wt% moganite. Considering the results of Moxon and Carpenter [23], these high moganite contents can be related to the geological age of the agates. However, it is noteworthy that the distribution of moganite within the silica matrix is not homogeneous. Raman mapping revealed extreme variations of the moganite content between different silica layers; particularly in zones with granular and macrocrystalline quartz, the moganite content approaches almost zero, whereas microcrystalline chalcedony contains elevated moganite contents (compare Figure 9).

The differences in moganite content are accompanied by variations in textural characteristics, including porosity (compare Figure 6). Therefore, the zoned distribution of moganite corresponds with the banded structure of the agates pointing to a multi-phase deposition of SiO_2. These structural and textural features strongly indicate variations in the physico-chemical conditions and a discontinuous silica supply.

6. Conclusions

The present study provides first detailed mineralogical data of agates from El Picado/Los Indios in the Eastern part of Cuba (Moa region). The investigations aimed to characterize the silica minerals in the agates and to provide data for the reconstruction of the agate forming processes.

The mineral composition of the agate-bearing Paleocene/Eocene tuffs is dominated by illite-smectite mixed-layer minerals, zeolites, opal-CT and calcite and has only minor amounts (<10 wt%) of residual primary plagioclase (andesine). These results document that the primary mineral composition of the predominantly SiO_2-poor, basic volcanic rocks is strongly modified during intensive secondary alteration. These surficial alteration processes must have caused the release of enormous amounts of aqueous silica that have been available for silicification processes and the formation of massive agates. Homogenization temperatures of fluid inclusions in macrocrystalline quartz (130–145 °C) point to the participation of hydrothermal fluids and/or heated meteoric water.

The mineral composition of the agates is dominated by alpha-quartz (microcrystalline chalcedony and macrocrystalline quartz), but also shows remarkable high abundances of moganite (>16 wt%) and opal-CT (>6 wt%). These elevated amounts of "immature" silica phases can probably be related to the geological age (~55 Ma) of the mineralization processes. The presence of opal-CT confirms the supposed formation of the agates via an amorphous silica precursor. Moreover, the heterogeneous distribution of moganite within the silica matrix, revealed by micro-Raman mapping as well as detected variations in the microtexture and porosity of the agates, indicate a multi-phase deposition of SiO_2 due to a discontinuous silica supply and probably varying physico-chemical conditions.

Author Contributions: K.S., G.O. and J.G. collected the studied samples and provided the geological data; J.G., T.M.-W. and M.L. conducted different analytical measurements, evaluated the mineralogical and spectroscopic data and provided appropriate parts of the manuscript; J.G. compiled and wrote the final version of the manuscript. All authors have read and agreed to the published version of the manuscript.

Funding: This research received no external funding.

Institutional Review Board Statement: Not applicable.

Informed Consent Statement: Not applicable.

Data Availability Statement: All data are contained within the article.

Acknowledgments: We would like to thank Reinhard Kleeberg (TU Bergakademie Freiberg, Germany) for assistance with XRD data acquisition and evaluation. Comments from Galina Palyanova (Novosibirsk, Russia) and the reviews of three anonymous reviewers improved the quality of the manuscript.

Conflicts of Interest: The authors declare no conflict of interest.

References

1. Barros de Oliveira, S.M.; De Moya Patiti, C.S.; Enzweiler, J. Ochreous laterite: A nickel ore from Punta Gorda, Cuba. *J. S. Am. Earth Sci.* **2001**, *14*, 307–317.
2. Gómez Narbona, L.J. Caracteristicas, usos, requisitos y metodos de evaluacion tecnologica de las manifestaciones de piedras preciosas Palmira, Loma de los Opalos, Pontezuela y Corralillo. In Proceedings of the IX Congreso Cubano de Geología (GEOLOGIA'2011), Influencia económica de la Microminería, La Habana, Cuba, 4–8 April 2011; pp. 1–11.
3. Moxon, T.; Palyanova, G. Agate genesis: A continuing enigma. *Minerals* **2020**, *10*, 953.
4. Götze, J.; Möckel, R.; Pan, Y. Mineralogy, geochemistry and genesis of agate—A review. *Minerals* **2020**, *10*, 1037.
5. Stanek, K.; Cobiella-Reguera, J.L.; Maresch, W.V.; Trujillo, G.M.; Grafe, F.; Grevel, C. Geological development of Cuba. *Z. Angew. Geol. Sonderh.* **2000**, *1*, 259–265.
6. Taut, T.; Kleeberg, R.; Bergmann, J. Seifert software: The new Seifert Rietveld program BGMN and its application to quantitative phase analysis. *Mater. Struct.* **1998**, *5*, 57–66.
7. Neuser, R.D.; Bruhn, F.; Götze, J.; Habermann, D.; Richter, D.K. Kathodolumineszenz: Methodik und Anwendung. *Zent. Geol. Paläontologie Teil I* **1995**, *H.1/2*, 287–306.
8. Graetsch, H. Structural characteristics of opaline and microcrystalline silica minerals. In *Silica—Physical Behaviour, Geochemistry and Materials Application*; Heaney, P.J., Prewitt, C.T., Gibbs, G., Eds.; Reviews in Mineralogy & Geochemistry; MSA: Washington, DC, USA, 1994; Volume 29, pp. 209–232.
9. Götze, J.; Blankenburg, H.-J. Zur Kathodolumineszenz von Achat—Erste Ergebnisse. *Der Aufschluß* **1994**, *45*, 305–312.
10. Kingma, K.J.; Hemley, R.J. Raman spectroscopic study of microcrystalline silica. *Am. Mineral.* **1994**, *79*, 269–273.
11. Götze, J.; Nasdala, L.; Kleeberg, R.; Wenzel, M. Occurrence and distribution of "moganite" in agate/chalcedony: A combined micro-Raman, Rietveld, and cathodoluminescence study. *Contrib. Mineral. Petrol.* **1998**, *133*, 96–105.
12. Natkaniec-Nowak, L.; Dumańska-Słowik, M.; Pršek, J.; Lankosz, M.; Wróbel, P.; Gaweł, A.; Kowalczyk, J.; Kocemba, J. Agates from Kerrouchen (The Atlas Mountains, Morocco). *Minerals* **2016**, *6*, 77.
13. Zhang, X.; Ji, L.; He, X. Gemological characteristics and origin of the Zhanguohong agate from Beipiao, Liaoning province, China: A combined microscopic, X-ray diffraction, and Raman spectroscopic study. *Minerals* **2020**, *10*, 401.
14. Götze, J.; Gaft, M.; Möckel, R. Uranium and uranyl luminescence in agate/chalcedony. *Mineral. Mag.* **2015**, *79*, 983–993.
15. Siegel, G.H.; Marrone, M.J. Photoluminescence in as-drawn and irradiated silica optical fibers: An assessment of the role of non-bridging oxygen defect centers. *J. Non-Cryst. Solids* **1981**, *45*, 235–247.
16. Stevens-Kalceff, M.A. Cathodoluminescence microcharacterization of point defects in α-quartz. *Mineral. Mag.* **2009**, *73*, 585–606.
17. Götze, J.; Plötze, M.; Habermann, D. Cathodoluminescence (CL) of quartz: Origin, spectral characteristics and practical applications. *Mineral. Petrol.* **2001**, *71*, 225–250.
18. Zielinski, R.A. Uranium mobility during interaction of rhyolitic obsidian, perlite and felsite with alkaline carbonate solution: T=120 °C, P=210 kg/cm^2. *Chem. Geol.* **1979**, *27*, 47–63.
19. Pan, Y.; Li, D.; Feng, R.; Wiens, E.; Chen, N.; Götze, J.; Lin, J. Uranyl binding mechanism in microcrystalline silicas: A potential missing link for uranium mineralization by direct uranyl co-precipitation and environmental implications. *Geochim. Cosmochim. Acta* **2021**, *292*, 518–531.
20. Dumańska-Słowik, M.; Natkaniec-Nowak, L.; Weselucha-Birczyńska; Gaweł, A.; Lankosz, M.; Wróbel, P. Agates from Sidi Rahal, in the Atlas Mountains of Morocco: Gemmological characteristics and proposed origin. *Gems Gemol.* **2013**, *49*, 148–159.
21. Götze, J.; Hofmann, B.; Machałowski, T.; Tsurkan, M.V.; Jesionowski, T.; Ehrlich, H.; Kleeberg, R.; Ottens, B. Biosignatures in subsurface filamentous fabrics (SFF) from the Deccan Volcanic Province, India. *Minerals* **2020**, *10*, 540.

22. Moxon, T.; Rios, S. Moganite and water content as a function of age in agate: An XRD and thermogravimetric study. *Eur. J. Mineral.* **2004**, *16*, 269–278.
23. Moxon, T.; Carpenter, M.A. Crystallite growth kinetics in nanocrystalline quartz (agate and chalcedony). *Mineral. Mag.* **2009**, *73*, 551–568.
24. Moxon, T. Agates: A study of ageing. *Eur. J. Mineral.* **2002**, *14*, 1109–1118.
25. Moxon, T. A re-examination of water in agate and its bearing on the agate genesis enigma. *Mineral. Mag.* **2017**, *81*, 1223–1244.